ADVANCED ENGINEERING MATERIALS
www.aem-journal.com

Tunable Mechanical Anisotropy, Crack Guiding, and Toughness Enhancement in Two-Stage Reactive Polymer Networks

Lewis M. Cox, Adrienne K. Blevins, Jasper A. Drisko, Yuan Qi, Yifu Ding, Callie I. Fiedler-Higgins, Rong Long, Christopher N. Bowman, and Jason P. Killgore*

Using simple and inexpensive processing methodologies afforded by two-stage reactive polymer networks (TSRPs) tunable mechanical anisotropy is displayed, defect-independent guiding of cohesive fracture paths through soft material is demonstrated for the first time, and bio-inspired microstructures are shown to enable performance enhancement beyond what is anticipated by the rule-of-mixtures in composites. The ability to pattern rubbery (stage I) and glassy (stage II) domains within a TSRP using photomasks and UV light is investigated through atomic force microscope (AFM) nanomechanical mapping techniques. AFM modulus mapping shows that the resulting stiffness anisotropy between stage I and stage II regions is length scale dependent. A gradient interface in elastic modulus between stage I and stage II materials is observed and, when patterned with an angled stage I pathway, the gradient interface exhibits remarkable resilience during failure, repeatedly deflecting cracks away from stage II regions, even while turning cracks at angles up to 135° When stage I and stage II domains are patterned in a nacre-inspired microstructure, toughening beyond rule-of-mixtures' prediction is observed.

Prof. L. M. Cox
Mechanical & Industrial Engineering Department
Montana State University
220 Roberts Hall, Bozeman, MT 59715, USA
E-mail: lewis.cox@montana.gov

Prof. L. M. Cox, Dr. J. P. Killgore, Dr. C. I. Fiedler-Higgins
Applied Chemicals and Materials Division
National Institute of Standards and Technology
325 Broadway, Boulder, CO 80305, USA

A. K. Blevins, Prof. Y. Ding, Prof. C. N. Bowman
Materials Science & Engineering Program
University of Colorado Boulder
4001 Discovery Drive, Boulder, CO 80303, USA

Dr. J. A. Drisko
Radio Frequency Technology Division
National Institute of Standards and Technology
325 Broadway, Boulder, CO 80305, USA

Y. Qi, Prof. Y. Ding, Prof. R. Long
Department of Mechanical Engineering
University of Colorado Boulder
1111 Engineering Drive, 427 UCB, Boulder, CO 80309, USA

DOI: 10.1002/adem.201900578

Photopolymers enable a vast range of applications such as low-cost rapid prototyping,[1] smart optics,[2] tunable surface topographies,[3–5] and tissue engineering for regenerative medicine.[6,7] In recent years, the importance of photopolymers has grown significantly as additive manufacturing (AM) techniques have enabled facile fabrication of three-dimensionally complex parts. A challenging goal of modern AM techniques, and photo-printed polymer parts in general, is controlling mechanical heterogeneity and interlayer adhesion in multi-material printed parts. Current methods for creating mechanical heterogeneity require exchange of precursor baths or extrusion filaments. In additively manufactured parts as well as traditional engineering composites, poor interfacial adhesion and interlayer bonding introduce mechanical weaknesses that concentrate stress and nucleate crack formation.[8,9] Printing spatially controlled mechanical heterogeneities with robust interfaces will provide a new degree of control within polymer and composite fabrication, allowing them to impact a range of applications such as soft robotics, flexible electronics, biomimetic materials, and consumer products.

An emerging class of photopolymers with the potential to create mechanically heterogeneous structures from a single resin are known as two-stage reactive polymer networks (TSRPs).[10] TSRPs are characterized by a two-step series of orthogonal reactions that enable spatial control over cross-linking density within a continuous polymer network. TSRPs employ a flexible "click" reaction[11] that polymerizes a liquid resin into a rubbery network (stage I) at ambient conditions while the subsequent free-radical photopolymerization transforms the material into a higher modulus glass (stage II). Previous work showed that the difference between the stage I and stage II material properties is easily tuned by altering the material formulation.[10] The processing methodology of TSRPs allows spatial patterning of rubbery and glassy domains. Recent work has demonstrated that both polymerization steps are spatially controlled using different wavelengths of light,[12] and stage II polymerization is carried out in as little as milliseconds,[13] positioning the material for integration into AM

platforms. Indeed, the very first AM platforms employing two wavelength's to print heterogeneous structures from a single resin vat by activating orthogonal polymerization reactions have recently been reported.[14,15] Despite standing on the precipice of widespread impact, the tunable and patternable mechanical behavior promised by TSRPs remains almost completely unexplored. Accordingly, in this work we demonstrate the flexibility in material performance obtainable in TSRP films using simple processing methodologies. Specifically, programmable mechanical anisotropy is investigated, defect-independent crack guiding through soft material is demonstrated for the first time, and bio-inspired microstructures are shown to enable performance enhancement beyond what is anticipated by the rule-of-mixtures. The results provide a framework to control mechanical performance of the next generation of photopolymers.

While numerous formulations are employed to synthesize TSRPs of different properties, here inexpensive and readily available monomers with a constant off-stoichiometry is used. We implement the thiol-acrylate Michael addition reaction[16–18] and employ a single monomer formulation to simplify characterization of mechanical performance. A multifunctional thiol, pentaerythritol tetrakis(3-mercaptopropionate) (PETMP), is mixed with a 1:2 functional group excess of trimethylolpropane triacrylate (TMPTA). Triethyl amine (TEA, 0.08 wt%) initiates a self-limiting, stoichiometric reaction between the thiol and acrylate functional groups, leaving the excess acrylate functional groups unreacted but covalently tethered to the polymer network,[10] **Figure 1**A. Measured at low frequency (1 Hz) the resulting material is a rubbery stage I film (thickness $t = 82 \pm 7\,\mu m$, Young's modulus $E = 2.5\,MPa \pm 1.3\,MPa$, glass transition temperature $T_g = -1\,^{\circ}C \pm 3\,^{\circ}C$) with properties determined by dynamic mechanical analysis (DMA, TA Instruments Q800).

Photoinitiator present in the stage I material (2,2-dimethoxy-2-phenylacetophenone, 1 wt%) is photocleaved with UV light to generate free radicals, initiating homopolymerization of the excess acrylate groups and generating a spatially controlled highly cross-linked stage II material ($E = 1.2\,GPa \pm 0.9\,GPa$, $T_g = 56\,^{\circ}C \pm 2\,^{\circ}C$), Figure 1B. Volumetric shrinkages in the range of 4% have been reported during stage II polymerization in TSRPs employing a 1:2 functional group excess.[19] Experimentally, we laminate the stage I films directly onto an etched-chrome photomask, place a neutral density filter on the opposite side of the film, and expose the film to UV light (300–400 nm wavelength, $10\,mW\,cm^{-2}$ intensity for 3 min) through the chrome mask, Figure 1C. An index matching oil (Type LDF, Cargille Labs) is layered between the underside of the film and the neutral density filter to mitigate phenomena that disrupt the ability to replicate the mask geometry onto the polymer film, such as light scattering, reflection, and oxygen diffusion since contact is not intimate between the film and filter.

Samples are cured using a photomask etched with 1:1 line-space grating patterns. To understand this phenomenon, spatially resolved mechanical properties of patterned TSRPs are investigated for the first time. An atomic force microscope (AFM, Cypher, Asylum Research) is used in fast force mapping (FFM) mode to measure the elastic modulus along the surface of the film after removing the photomask. AFM modulus measurements are analyzed using a Hertzian contact mechanics model. Line-space patterns with widths of 100, 10, and 5 μm are used during exposures and the resulting AFM scans show distinct, mechanical heterogeneity with micron-scale pattern resolution, **Figure 2**A (color bars presented in log-scale throughout the paper). Modulus variations moving from the UV-exposed, stage II region to the unexposed regions are plotted in Figure 2B. The elastic modulus of the stage I domain is measured at an elevated frequency in FFM and is 9.7 ± 0.3 MPa,

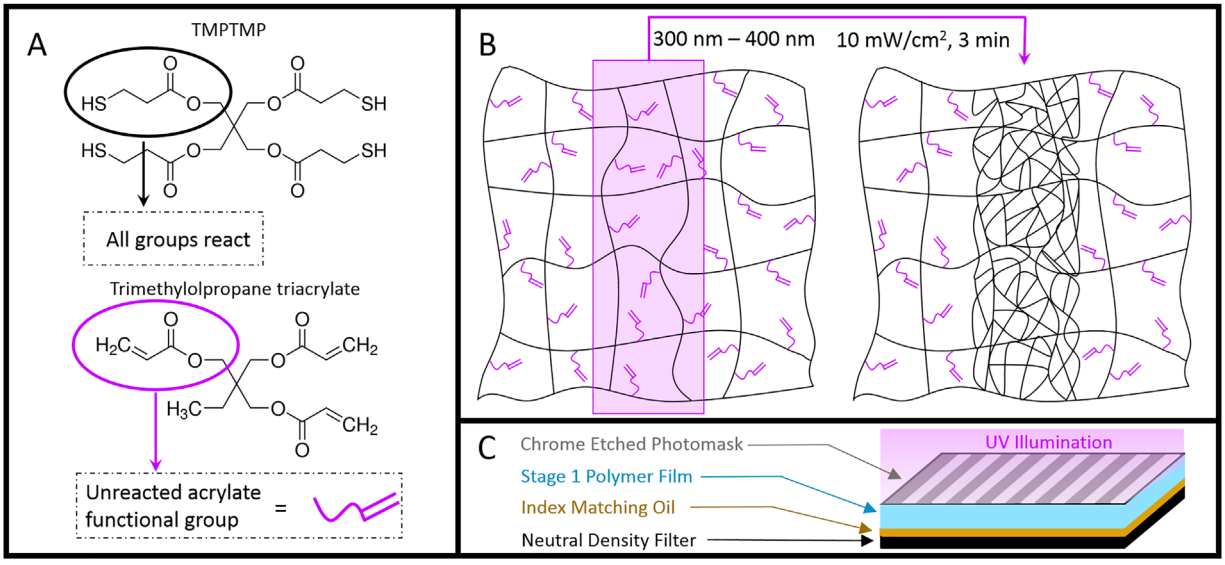

Figure 1. A) The oligomer precursors PETMP and TMPTA are mixed with a 2:1 acrylate:thiol functional group off stoichiometry. After TEA-mediated polymerization has completed, the excess, unreacted acrylate groups remain tethered to the network (B) that can be subsequently free-radical homopolymerized upon UV exposure, with spatial control (C), using the photoinitiator DMPA.

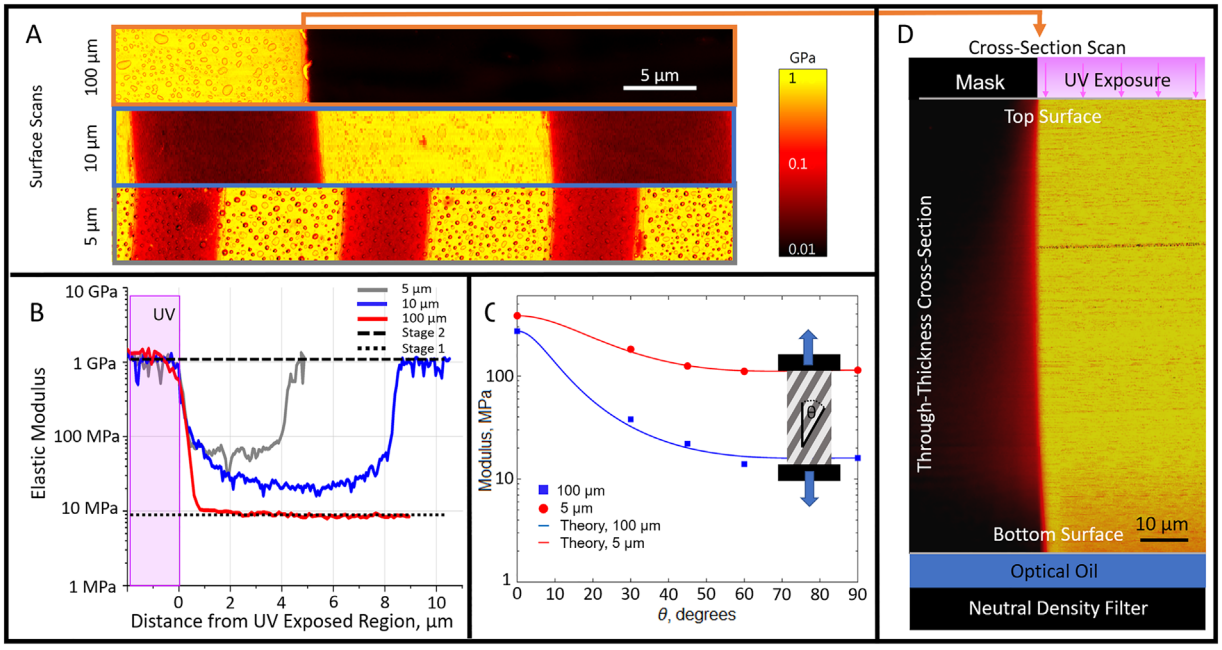

Figure 2. A) AFM fast force mapping of films after photopatterning shows clear elastic modulus patterns along the film surface. B) The modulus profiles moving between the UV-exposed and mask-shaded areas are dependent upon the pattern length scale. C) Line patterns are oriented at various angles relative to the loading direction and compared to theoretical predictions, demonstrating clear anisotropy. D) Film cross-sections exhibit good pattern uniformity throughout the thickness of the film. Color scale corresponds to both **(A)** and **(D)**.

which differs from the Young's modulus reported above, but is in line with 100 Hz DMA measurements of storage modulus, Table S1, Supporting Information. The 1:1 line:space mask pattern is not perfectly replicated on the surface as the 10 and 5 μm patterns exhibit a line-broadening effect with 1:0.8 and 1:0.7 line:space ratios, respectively. Notably, the moduli in the masked areas are dependent upon the length scale of the pattern. As the pattern size shrinks, the elastic modulus in the areas shaded by the chrome mask increases. A multiple order-of-magnitude variation in modulus is achieved across the 100 μm patterns, where the shaded areas retain the initial stage I modulus during and after the stage II regions' exposure. This contrasts with the single-order-of-magnitude variation seen across the 5 μm pattern, indicating that partial polymerization has occurred in the masked area, resulting in a leathery intermediate material. This phenomenon is attributed to the increased rates of O_2 gas consumption as smaller features are employed. Oxygen inhibits free radical acrylate homopolymerization through radical scavenging.[20,21] Increasing the surface area of interfaces between exposed and shaded regions results in more rapid consumption of oxygen throughout the network. This consumption, in turn, enables minor amounts of light scattering and free radical diffusion to partially cure shaded regions. Orienting the line-patterned films at various angles relative to a tensile load in a dynamic mechanical analyzer (DMA) and measuring stiffness, anisotropy is readily observed, Figure 2C. Laminate theory, Equations (S1)–(S4), forces agreement at orientation angles of 0° and 90°, and shows excellent prediction of material behavior at the intermediate angles. Following Equations (S1)–(S6), the anisotropic response could be tuned by modulating the volume fraction of the two phases through changes to the line:space ratio.

An important feature of Figure 2B is the manifestation of a 1 to 2 μm modulus gradient spanning the interface between the exposed and shaded areas. Formation of an interface at this length scale is likely due to shrinkage of the illuminated domains during the second stage free-radical polymerization, the same phenomenon affecting the fidelity of replication of the mask geometry. In traditional engineering composites the interface between material phases present physical discontinuities in elastic modulus that concentrate stress and act as a primary locus for structural failure.[9,22,23] This ubiquitous weakness is clearly absent in patterned TSRP heterostructures leading to benefits illustrated later in this work. In macroscopic systems, interfaces toughened through interpenetration of mechanically heterogeneous networks has demonstrated crack trapping capabilities that impart fatigue resistance not dependent upon energy dissipation.[24] While the term "interface" is applied to TSRPs throughout this manuscript, it should be noted its usage is unusual. Despite the emergence of clear mechanical heterogeneity, the entire TSRP heterostructure is comprised of one large, covalently interconnected molecule, as is typical of thermosets. Interface is used here to describe the spatial transitions in mechanical properties within a single molecular network. To evaluate the uniformity of these surface patterns throughout the thickness of the film, a cryo-ultramicrotome (Leica, EM FC7) is used to generate a flat cross-section of the films required for accurate FFM. FFM measurements performed on the cross-section of the 100 μm line-space pattern show that this simple processing methodology provides good pattern uniformity

throughout the film's volume, Figure 2D. Film thickness is kept at this length scale throughout the work to facilitate AFM characterization of heterogeneities throughout film volumes. While previous work has shown UV curing of stage II materials can extend to macroscopic length scales,[10] evolution of this interface morphology at macroscopic depths remains an open area of interest.

With spatial modulus control and a gradient interface, TSRPs offer a new paradigm to control material failure in addition to elastic response. In soft materials the study of crack propagation,[25–29] instabilities,[30,31] and deflection[32] has advanced considerably in recent years, but guiding cohesive failure along predetermined pathways is elusive in soft matter. In rigid materials crack guiding phenomenon has been demonstrated, but requires the controlled generation of structural defects.[33,34] In contrast, biomaterials with three-dimensional material structure, such as glass sponges, leverage the ability to impose tortuous crack pathways as a toughening mechanism.[35,36] Here, TSRPs exhibit the ability to guide cohesive failure along predetermined pathways for the first time in soft materials, without the need for defect introduction. Rubbery pathways, 1 mm wide with turn angles ranging from 60° to 135° are patterned with corresponding photomasks (inset **Figure 3**A), which results in successful crack guiding along each of the engineered pathways, Figure S2, Supporting Information. No pre-crack is implemented and failure spontaneously nucleates and propagates within the stage I pathways. The extreme of these experiments, which creates a stage I pathway executing a 135° turn as it bisects an otherwise stage II sample, is shown in Figure 3A, photomask inset. A static strain ramp of 3%/min, loading vertically with respect to the orientation of Figure 3A, is imposed until sample failure. The results present a novel degree of control over fracture topology in a continuous polymer network. For context, crack deflection and bifurcation have been shown to turn cracks at angles near 90° in soft materials,[32] but this degree of crack angling has never been demonstrated under unidirectional loading conditions. Interestingly, even if a notch is introduced into the glassy, stage II region above the stage I pathway, when loaded in tension the crack quickly propagates into the stage I pathway and continues guiding as for unnotched cases, Figure S3, Supporting Information.

FFM along the fracture path shows that Mode I failure remains within the stage I material and avoids contacting the interface even when it rounds the lower corner of the pathway, Figure 3B. Once the crack reaches the back edge of the stage I pathway angled at 135°, it propagates toward the interface, is arrested and moves back out prior to ever contacting the stage II material, Figure 3C, a phenomenon that repeats until the top corner is navigated by the crack. This mixed-mode failure creates a scalloped fracture surface with small cracks projecting outward from the scallop apex towards the interface. Strikingly, the projected crack remains fully inside the rubbery stage I material and, while the scallop morphology varies slightly along the interface, the crack is never observed to reach within 2.5 μm of the interface edge, where the modulus begins to rise. The way dissipative regimes interact with mechanical heterogeneities and enable cracks to "sense" structure at a distance is poorly understood and Figure 3C provides a unique visualization of this phenomenon.[28] The absence of crack nucleation or entrenchment along the interface throughout the guiding behavior highlights the robustness of the continuous interface. Weak interfaces present in traditional engineering hybrid structures and all layer-by-layer additive manufacturing techniques serve as a primary locus for crack nucleation and entrenchment, a phenomenon which is circumvented here and can be leveraged as acrylate resins continue to be developed for additive manufacturing techniques.[37–39] The ability to guide cohesive failure along complex pathways enables predictability of crack nucleation zones, failure modes, and control over fracture topology.

This crack guiding behavior is governed by intrinsic material properties (e.g., fracture toughness, failure stress) as well as structural effects (e.g., geometry, loading conditions). If the width of the rubbery pathway were negligible with respect to the overall path geometry, the ability to guide cracks would be completely governed by intrinsic material properties, modeled as,[33]

$$\cos^2\frac{\theta}{2} > \frac{K_{IC}^{\text{Stage 1}}}{K_{IC}^{\text{Stage 2}}} \tag{1}$$

where θ is an arbitrary guiding angle and K_{IC} is the fracture toughness of the two homogeneous material stages present in the heterostructure. This criterion indicates that a crack can be expected to follow an angled pathway if its fracture toughness is sufficiently lower than that of the surrounding media. However, as the width of the programmed pathway is 1 mm, variations in the stress field will evolve as the crack propagates. These variations have been modeled and used to simulate crack propagation through the rubbery pathway under the assumption that the crack moves perpendicular to the direction of maximum principal stress, Figure 3D (modeling details in Supporting Information). The model captures how variations in the stress field guide the crack through initial stages of propagation, including the bend around the lower corner. Upon approaching the back edge of the rubbery pathway, Figure 3C, a complex interplay between the extrinsic structural effects and intrinsic material properties arise and no theory exists to adequately model this behavior.[28] TSRPs offer a new platform to provide insights to complex fracture phenomena.

Additional control of structural failure throughout the 135° pathway is obtained by engineering complex mechanical heterogeneity through the film thickness. Through-thickness structural variation is achieved by modifying material formulation and processing conditions during UV illumination. To achieve a through-thickness modulus gradient, 0.4 wt% photoinhibitor (Tinuvin 328, BASF) is added to the formulation. The final structure is comprised of a stage II modulus at the top of the film that gradually decreases through the thickness until the stage I modulus is reached at the bottom of the film, the resulting photoinhibited gradient (PIG) in modulus obtained from FFM along the cross-section is shown in Figure 3E. Further structural complexity is obtained without such modifications to material formulation by altering boundary conditions around the film during UV exposure. For example, introducing an air gap between the lower surface and the neutral density filter results in significantly more light scattering and reflection, enabling light to reach volumes shaded from UV exposure by the

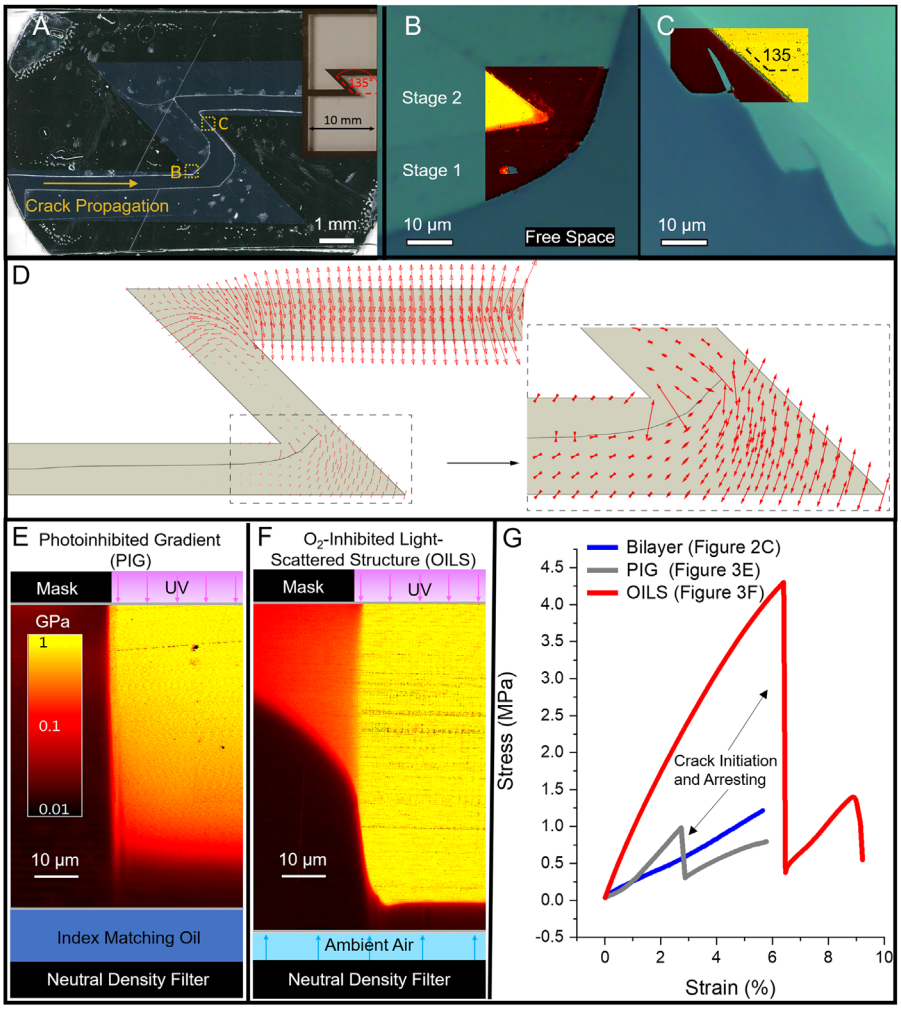

Figure 3. A) A crack nucleates within the stage I domain and is guided through a photopatterned pathway with a 135° turn angle. B) FFM map overlaid on an optical image shows how Mode 1 fracture propagates laterally without becoming entrenched along the mechanical interface and navigate around the turn angle. C) The crack oscillates towards and away from the interface as it climbs the back turn of the Stage I pathway exhibiting jagged, mixed mode failure that avoids contacting the Stage II material. D) A snapshot of crack growth in the Stage 1 material. Red arrows represent the direction and magnitude of the principal stress. Initially, crack propagates horizontally due to the nearly uniform and vertical maximum principal stress. When it approaches the 135-degree corner, the distribution of the maximum principal stress, determined by the local geometry, causes the crack path to bend upwards. E) Control over material composition and structure through the thickness of the film is achieved by photoinhibition, generating a gray-scale modulus that gradually transitions from a Stage II material to a Stage I material. More complex through-thickness structure can be realized by implementing an air gap along the lower surface of the film, allowing enhanced light scattering and oxygen inhibition to generate complex three-phase modulus profiles both in exposed and masked regions (F). The more complex grayscale and three-phase profiles manifest a crack arrest phenomenon that is not observed in the simple bilayer system (G). Color bar applies to (B) through (F).

photomask. Additionally, the gap facilitates oxygen diffusion into the polymer network, which inhibits free radical polymerization throughout regions within the film.[38,40] The through-thickness modulus of the resulting O_2-inhibited light-scattered structure (OILS) is displayed in Figure 3F. In this sample, volumes directly exposed to UV achieve a glassy, stage II modulus through most of the film thickness, but within 8 μm of the bottom surface oxygen inhibits the acrylate homopolymerization, maintaining a thin layer of stage I material. In shaded volumes, partial homopolymerization is indicated by the presence of leathery material with a modulus on the order of 100 MPa. The intensity of light in shaded regions is significantly lower than in exposed regions, reducing reaction rates and allowing oxygen to diffuse farther into the network, inhibiting polymerization. The greater the distance from regions where UV penetrates the film, the further away from the lower surface oxygen can inhibit polymerization in shaded regions, creating the concave stage I shape in Figure 3F. The architectures presented here offer unique abilities to interact with and control the paths of propagating cracks. Compared with the previously presented bilayer structure, which undergoes a rapid, guided failure around the 135° turn after crack nucleation, both the PIG and OILS architectures demonstrate crack arresting behavior, while still successfully guiding the crack path, Figure 3G. After crack

nucleation, there is a period of rapid lateral translation until the crack encounters the back edge of the 135° angled pathway, at which point the arresting phenomenon is observed until the displacement becomes such that the crack slowly propagates along the angled portion of the pathway and rounds the top corner, where rapid lateral translation again occurs. The three-phase structure exhibits a significantly higher effective stiffness than the other two structures during tensile loading as the crack pathway bisecting the structure is no longer a pure stage I material and is spanned by the higher modulus, leathery material.

In modern advanced materials a key challenge, beyond control of fracture topology, is leveraging structural control to extrinsically toughen materials and outperform rule-of-mixtures predictions from the constituent phases.[41,42] A natural example of such performance enhancement is nacre, a biomaterial that possesses a tessellated brick-and-mortar structure that imparts defect tolerance and crack shielding mechanisms, resulting in a fracture toughness orders of magnitude greater than its constitutive components.[43–45] Here, a photomask etched with a nacre-inspired, brick and mortar pattern similar in structure to geometries used in existing literature,[46] **Figure 4**A, is used to process the TSRP. Bricks are represented by white space and the mortar by the black line. Mortar represents 8% of the shaded area fraction of the mask pattern and, per Figure 2D, it is reasonable to extrapolate this as the resulting volume fraction in cured films. The bricks correspond to UV-exposed areas and the mortar corresponds to masked areas. Bricks in the resulting films are comprised of stage II TSRP material and have a 1° flare angle to mimic the natural waviness of nacre bricks. The length scale of the pattern is varied in separate specimens and the overall tensile toughness and Young's modulus are determined, Figure 4B. Tensile toughness, calculated as area under the stress vs strain curve, is reported in lieu of traditional fracture toughness. We report in this manner since the length scale of heterogeneous patterns is significantly larger than the 16 μm radius of curvature of a crack tip just before propagation, estimated from[28]

$$\rho \approx G_c/E \tag{2}$$

where G_c and E are the Mode-I fracture energy and Young's modulus of the stage I material (Table S1), leaving us unable to justify the assumption of homogeneity necessary for fracture toughness calculations. Depicted in Figure 4A, the tensile load is applied along the length of the bricks. As initially presented in Figure 2A and B, the modulus of the shaded (mortar) regions is dependent upon the length scale of the features and the mortar in the smallest patterns has a significantly higher modulus than the mortar in the larger pattern geometries. Accordingly, there are four different rule-of-mixture predictions drawn in Figure 4B that connect the performance of the monolithic stage II bricks to the properties of the mortar material relevant to the pattern length scale. Monolithic samples with similar material properties to the mortar are obtained by partially curing stage I films with varied UV exposure times and subjecting them to static strain tensile ramps to obtain toughness values. Patterned data that falls below the line of similar color (e.g., red triangle corresponds with red line) underperform the rule-of-mixtures, while data residing above its respective line exceeds rule-of-mixture's prediction. For the two largest pattern sizes where the brick lengths (L) are 2 and 1 mm the mortar is comprised of the compliant stage I material, which exhibits both an inferior toughness and Young's modulus compared to the stage II bricks. The two resulting patterned materials greatly underperform the rule-of-mixtures, exhibiting only 16 and 18% of the toughness anticipated for their respective Young's moduli. For patterns with brick lengths of 0.4 and 0.2 mm the mortar lines are 10 and 5 μm wide, respectively, which imparts the elevated moduli of leathery intermediates shown in Figure 2A and B. The smallest pattern size presents the only structure able to outperform the rule-of-mixtures, producing a toughness that is 185% of the

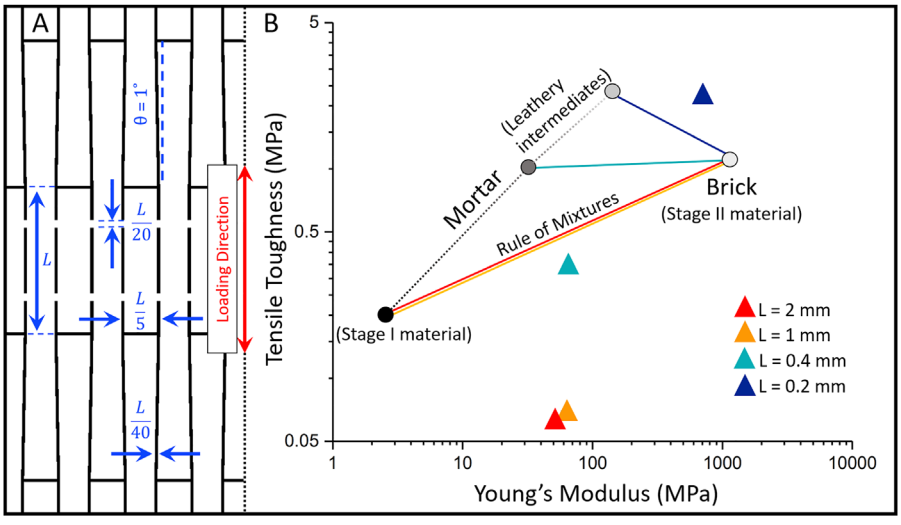

Figure 4. A) Tessellated brick-and-mortar patterns inspired by nacre are patterned into films using varied length scales. B)The resulting toughness is compared to the values anticipated by composite rule-of-mixtures, acknowledging that the material properties of the mortar will vary depending on the pattern length scale.

anticipated value. Two factors likely bolstering the performance of the smallest pattern size are the brick aspect ratios and the pattern size relative to the length scale of potential crack tips. Regarding the former, the photomask pattern is scaled down proportionally, but the film (and therefore brick) thickness remains constant. Previous work has shown the thickness of the bricks can greatly impact material performance.[46] The overall size of the smallest pattern may drop to a length scale similar to that of a potential crack tip radius. This would facilitate crack bridging, a toughening mechanism known to reduce stress concentrations around cracks and defects present in similarly structures materials.[47] It is clear that tessellated structural patterns are either detrimental or advantageous to material performance and that the flexible processing underlying TSRPs provides a unique platform for further investigations into this phenomenon.

In conclusion, the control over mechanical performance offered by TSRPs is impressive, especially considering the processing simplicity. We report patterning with increasing complexity from line-gratings, to angles, to a bio-inspired nacre-like structure, with separate control over the through-thickness heterogeneity also possible. When printing line-grating patterns, the resulting stiffness anisotropy was found to be length scale dependent. Nanomechanical mapping indicated a modulus gradient interface between stage I and stage II materials, with a higher degree of cure in the masked regions of smaller pattern features versus larger. When patterned with an angled stage I pathway, the gradient interface exhibited remarkable resilience during failure, repeatedly deflecting cracks away from stage II, even at angles up to 135°. Such large angle guiding has never been achieved in the cohesive fracture of soft materials. By tuning the through-thickness conversion of the polymer, leathery intermediate domains were introduced, resulting in crack arresting behavior and enhanced toughness at the same 135° angle. The programmed heterogenieties are then incorporated into a nacre-inspired tessellated brick-and-mortar microstructure. Varying the size of the pattern features allowed for toughening beyond rule-of-mixtures' prediction when the smallest pattern features were employed. Moving forward, TSRPs provide a novel system for scientific investigation of fracture in heterogenous structures without the hindrance of crack nucleation or entrenchment along weak interfaces. The facile programming of heterogeneity and accompanying resilient interfaces can be leveraged to optimize fracture and performance of future acrylate photopolymers as they are developed.

Experimental Section

Film Synthesis: Pentaerythritol tetrakis(3-mercaptopropionate) (PETMP) is mixed with a 1:2 functional group excess of trimethylolpropane triacrylate (TMPTA). Triethyl amine (TEA, 0.08 wt%) is used as the catalyst for the first stage reaction and the photoinitiator 2,2-Dimethoxy-2-phenylacetophenone (DMPA, 1 wt%) is used to initiate the second stage reaction. Both TEA and DMPA were dissolved in PETMP prior to mixing with TMPTA. After adding TMPTA the mixture was vigorously stirred for several minutes, then cast onto glass slides and allowed to cure overnight. While nucleophilic catalysts have been shown to initiate and complete the Michael addition reaction quickly and efficiently, TEA was chosen for the control it affords over the initial rate of the reaction,[15] allowing more processing time to cast the mixture.

Supporting Information

Supporting Information is available from the Wiley Online Library or from the author.

Acknowledgements

This work was performed while Lewis Cox and Callie Fiedler-Higgins held National Research Council Associateship Awards at NIST. Contribution of NIST, an agency of the U.S. government; not subject to copyright in the United States. Commercial equipment, instruments, or materials are identified only in order to adequately specify certain procedures. In no case does such identification imply recommendation or endorsement by the National Institute of Standards and Technology, nor does it imply that the products identified are necessarily the best available for the purpose. The authors would like to thank Benjamin W. Caplins for his insightsand support with image processing.

Conflict of Interest

The authors declare no conflict of interest.

Keywords

two-stage reactions, photopolymerization, thiol-acrylate, crack guiding

Received: May 15, 2019
Published online:

[1] B. Berman, *Business Horizons* **2012**, *55*, 155.
[2] M. K. McBride, M. Hendrikx, D. Liu, B. T. Worrell, D. J. Broer, C. N. Bowman, *Adv. Mater.* **2017**, *29*, 1606509.
[3] B. T. Worrell, M. K. McBride, G. B. Lyon, L. M. Cox, C. Wang, S. Mavila, C.-H. Lim, H. M. Coley, C. B. Musgrave, Y. Ding, C. N. Bowman, *Nat. Commun.* **2018**, *9*, 2804.
[4] L. M. Cox, X. Sun, C. Wang, N. Sowan, J. P. Killgore, R. Long, H.-A. Wu, C. N. Bowman, Y. Ding, *ACS Appl. Mater. Interfaces* **2017**, *9*, 14422.
[5] M. K. McBride, A. M. Martinez, L. Cox, M. Alim, K. Childress, M. Beiswinger, M. Podgorski, B. T. Worrell, J. Killgore, C. N. Bowman, *Sci. Adv.* **2018**, *4*, eaat4634.
[6] H. Cui, M. Nowicki, J. P. Fisher, L. G. Zhang, *Adv. Healthcare Mater.* **2017**, *6*, 1601118.
[7] M. S. Mannoor, Z. Jiang, T. James, Y. L. Kong, K. A. Malatesta, W. O. Soboyejo, N. Verma, D. H. Gracias, M. C. McAlpine, *Nano Lett.* **2013**, *13*, 2634.
[8] O. S. Es-Said, J. Foyos, R. Noorani, M. Mendelson, R. Marloth, B. A. Pregger, *Mater. Manuf. Process.* **2000**, *15*, 107.
[9] S.-Y. Fu, X.-Q. Feng, B. Lauke, Y.-W. Mai, *Compos. Part B-Eng.* **2008**, *39*, 933.
[10] D. P. Nair, N. B. Cramer, J. C. Gaipa, M. K. McBride, E. M. Matherly, R. R. McLeod, R. Shandas, C. N. Bowman, *Adv. Funct. Mater.* **2012**, *22*, 1502.
[11] C. E. Hoyle, C. N. Bowman, *Angew. Chem. Int. Ed.* **2010**, *49*, 1540.
[12] X. Zhang, W. Xi, S. Huang, K. Long, C. N. Bowman, *Macromolecules* **2017**, *50*, 5652.

[13] C. I. Fiedler-Higgins, L. M. Cox, F. W. DelRio, J. P. Killgore, *Small Methods* **2019**, *3*, 1800275.
[14] J. J. Schwartz, A. J. Boydston, *Nat. Commun.* **2019**, *10*, 791.
[15] N. D. Dolinski, Z. A. Page, E. B. Callaway, F. Eisenreich, R. V. Garcia, R. Chavez, D. P. Bothman, S. Hecht, F. W. Zok, C. J. Hawker, *Adv. Mater.* **2018**, *30*, 1800364.
[16] J. W. Chan, C. E. Hoyle, A. B. Lowe, *J. Am. Chem. Soc.* **2009**, *131*, 5751.
[17] J. W. Chan, C. E. Hoyle, A. B. Lowe, M. Bowman, *Macromolecules* **2010**, *43*, 6381.
[18] B. D. Mather, K. Viswanathan, K. M. Miller, T. E. Long, *Progr. Polym. Sci.* **2006**, *31*, 487.
[19] H. Peng, D. P. Nair, B. A. Kowalski, W. Xi, T. Gong, C. Wang, M. Cole, N. B. Cramer, X. Xie, R. R. McLeod, C. N. Bowman, *Macromolecules* **2014**, *47*, 2306.
[20] K. Studer, C. Decker, E. Beck, R. Schwalm, *Progr. Organic Coat.* **2003**, *48*, 92.
[21] T. Y. Lee, C. A. Guymon, E. S. Jönsson, C. E. Hoyle, *Polymer* **2004**, *45*, 6155.
[22] S. Sun, C. Li, L. Zhang, H. L. Du, J. S. Burnell-Gray, *Eur. Polym. J.* **2006**, *42*, 1643.
[23] N. Sowan, L. M. Cox, P. K. Shah, H. B. Song, J. W. Stansbury, C. N. Bowman, *Adv. Mater. Interfaces* **2018**, *5*, 1800511.
[24] Z. Wang, C. Xiang, X. Yao, P. L. Floch, J. Mendez, Z. Suo, *PNAS* **2019**, *116*, 5967.
[25] N. P. Mitchell, V. Koning, V. Vitelli, W. T. M. Irvine, *Nat. Mater.* **2017**, *16*, 89.
[26] B. N. J. Persson, O. Albohr, G. Heinrich, H. Ueba, *J. Phys. Condens. Matter* **2005**, *17*, R1071.
[27] E. Ducrot, Y. Chen, M. Bulters, R. P. Sijbesma, C. Creton, *Science* **2014**, *344*, 186.
[28] C. Creton, M. Ciccotti, *Rep. Prog. Phys.* **2016**, *79*, 046601.
[29] F. Luo, T. L. Sun, T. Nakajima, T. Kurokawa, Y. Zhao, A. B. Ihsan, H. L. Guo, X. F. Li, J. P. Gong, *Macromolecules* **2014**, *47*, 6037.
[30] P. M. Reis, A. Kumar, M. D. Shattuck, B. Roman, *EPL* **2008**, *82*, 64002.
[31] S. Moulinet, M. Adda-Bedia, *Phys. Rev. Lett.* **2015**, *115*, 184301.
[32] H. Guo, N. Sanson, D. Hourdet, A. Marcellan, *Adv. Mater.* **2016**, *28*, 5857.
[33] M. Mirkhalaf, A. K. Dastjerdi, F. Barthelat, *Nat. Commun.* **2014**, *5*, 3166.
[34] K. H. Nam, I. H. Park, S. H. Ko, *Nature* **2012**, *485*, 221.
[35] J. Aizenberg, J. C. Weaver, M. S. Thanawala, V. C. Sundar, D. E. Morse, P. Fratzl, *Science* **2005**, *309*, 275.
[36] P. Fratzl, H. S. Gupta, F. D. Fischer, O. Kolednik, *Adv. Mater.* **2007**, *19*, 2657.
[37] M.-Y. He, J. W. Hutchinson, *J. Appl. Mech.* **1989**, *56*, 270.
[38] J. R. Tumbleston, D. Shirvanyants, N. Ermoshkin, R. Janusziewicz, A. R. Johnson, D. Kelly, K. Chen, R. Pinschmidt, J. P. Rolland, A. Ermoshkin, E. T. Samulski, J. M. DeSimone, *Science* **2015**, *347*, aaa2397.
[39] J. E. Seppala, S. H. Han, K. E. Hillgartner, C. S. Davis, K. B. Migler, *Soft Matter* **2017**, *13*, 6761.
[40] D. Dendukuri, P. Panda, R. Haghgooie, J. M. Kim, T. A. Hatton, P. S. Doyle, *Macromolecules* **2008**, *41*, 8547.
[41] H. T. Hahn, S. W. Tsai, *Introduction to Composite Materials*, CRC Press, Boca Raton, FL USA **1980**.
[42] R. O. Ritchie, *Nat. Mater.* **2011**, *10*, 817.
[43] U. G. K. Wegst, H. Bai, E. Saiz, A. P. Tomsia, R. O. Ritchie, *Nat. Mater.* **2015**, *14*, 23.
[44] A. P. Jackson, J. F. V. Vincent, R. M. Turner, *Proc. R. Soc. Lond. B* **1988**, *234*, 415.
[45] F. Barthelat, H. D. Espinosa, *Exp. Mech.* **2007**, *47*, 311.
[46] H. D. Espinosa, A. L. Juster, F. J. Latourte, O. Y. Loh, D. Gregoire, P. D. Zavattieri, *Nat. Commun.* **2011**, *2*, 173.
[47] X. Q. Li, H. C. Zeng, *Adv. Mater.* **2012**, *24*, 6277.
[48] H. Tada, P. C. Paris, G. R. Irwin, *The Stress Analysis of Cracks Handbook*, 3rd ed., ASME, Three Park Avenue New York, NY 10016–5990, **2000**.
[49] V. V. Vasiliev, E. V. Morozov, *Advanced Mechanics of Composite Materials and Structures* (Eds.: V. V. Vasiliev, E. V. Morozov), 4th ed., Elsevier, Amsterdam, Netherlands the **2018**, pp. 1–73.

